ADVANCED FUNCTIONAL MATERIALS
www.afm-journal.de

Superparamagnetic Ag@Co-Nanocomposites on Granulated Cation Exchange Polymeric Matrices with Enhanced Antibacterial Activity for the Environmentally Safe Purification of Water

*Amanda Alonso, Xavier Muñoz-Berbel, Núria Vigués, Rosalía Rodríguez-Rodríguez, Jorge Macanás, Maria Muñoz, Jordi Mas, and Dmitri N. Muraviev**

Cation exchange polymeric matrices are widely used in water treatment protocols to reduce the mineral content of hard waters, even for human consumption. However, they are not antibacterial and flowing bacteria can be trapped in their structures and proliferate, thus acting as microbial contamination sources. Here, Ag@Co-nanoparticles (Ag@Co-NPs) with a low-cost superparamagnetic Co^0-core and an antibacterial Ag-shell are synthesized on granulated cation exchange polymeric matrices under soft reaction conditions. The presence of these NPs provides the final nanocomposite (NC) with additional functionalities (superparamagnetism and antibacterial activity) making it ideal for water purification applications. Ag@Co-NPs are synthesized in situ on four cation exchange polymeric matrices containing either strong (sulfonic) or weak (carboxylic) acid functional groups homogeneously distributed (C-type) or concentrated on an external shell (SST-type) by the intermatrix synthesis (IMS) method. The NCs are characterized (metal content, NP size and distribution, metal oxidative state, and metal release) and evaluated for water purification applications.

1. Introduction

The requirement of safe water for livestock, food production, and energy is enormous and is expected to increase with the population growth. This huge demand and the limited natural water resources make the access to potable water one of the major concerns worldwide nowadays.[1] Only considering human consumption, millions of people around the world die or become ill due to lack of potable water, especially in China, India, and Southeast Asia.[2] On the other hand, the contamination of water supplies traditionally considered clean (e.g., water sources and aquifers) in industrialized and developing countries, the reduction of snowmelt and the loss of glaciers may limit the future access to potable water even in North America and Europe.[3] Future actions to mitigate this are focused on the development of suitable water treatment protocols for water disinfection, decontamination, and desalinization.[1] From all contaminants present in impaired waters, microorganisms are the ones with a highest social, sanitary, and economical impact.[4] Microbial contamination of water sources is commonly eliminated with intensive and continuous chemical treatments, mainly with chlorine compounds or ozone. However, the continuous production of residual chemicals in the water distribution systems[5] and the emergent presence of microorganisms resistant to multiple antimicrobial agents[6] recommend the development of alternative purification methods. Silver, silver colloids, and more recently silver nanoparticles (Ag-NPs) have been positioned as potential alternatives to the traditional disinfection methods for being highly effective against Gram-positive and Gram-negative bacteria and produce fewer residues.[7] However, one of the main concerns about using Ag-NPs for water purification is their toxicity since Ag-NPs have been found more toxic than bulk silver.[8] The main strategy to prevent the post-contamination of samples treated with Ag-NPs consists of using stabilizers (e.g., functionalized polymers) to retain the NPs on their structure.[9] Interesting examples are the hydrogel-silver

Dr. A. Alonso, Prof. M. Muñoz, Prof. D. N. Muraviev
Department of Chemistry
Universitat Autonòma de Barcelona (UAB)
Bellaterra, Barcelona, 08913, Spain
E-mail: dimitri.muraviev@uab.cat
Dr. X. Muñoz-Berbel
Centre Nacional de Microelectrònica (IMB-CNM, CSIC)
Bellaterra, Barcelona, 08913, Spain
N. Vigués, Prof. J. Mas
Department of Genetics and Microbiology
Universitat Autonòma de Barcelona (UAB)
Bellaterra, Barcelona, 08913, Spain
Dr. R. Rodríguez-Rodríguez
Department of Pharmacology
School of Pharmacy
Universidad de Sevilla (US)
Sevilla, 41004, Spain
Dr. J. Macanás
Department of Chemical Engineering
Universitat Politècnica de Catalunya (UPC)
Terrassa, 08222, Spain

DOI: 10.1002/adfm.201202663

nanoparticle composites presented by Varaprasad et al.[10] or the agar-agar matrix used by Ghosh et al.[11] to stably immobilize Ag-NPs. With these materials, the number of Ag-NPs released during the treatment is low but still persistent, thus limiting their application to water purification. One alternative to solve it is the selective collection of the released NPs with non-invasive methods that do not modify the quality of the treated water. Based on it, some groups have synthesized core-shell NPs or nanocomposites (NCs) with magnetic and antibacterial activity, which, in case of being released from the matrix, could be easily collected with a simple magnet.[12] This additional safety level is essential for their application to real-life water purification systems.

Here, Ag@Co-NPs with a low-cost superparamagnetic Co^0-core and an antibacterial Ag-shell are synthesized in situ under soft reaction conditions (short reaction times and low temperatures) on granulated cation exchange polymeric matrices for water purification applications. Cation exchange polymeric matrices are commonly used in water treatment protocols to reduce the mineral content of hard waters, even for human consumption. However, because they are not antibacterial, bacteria can be retained and proliferate, thus acting as microbial contamination sources. The presence of antibacterial Ag@Co-NPs on the cation exchange polymeric matrix reduces bacterial viability and contamination problems. Ag@Co-NPs are synthesized in situ on four cation exchange polymeric matrices containing either strong (sulfonic) or weak (carboxylic) acid functional groups homogeneously distributed (C-type) or concentrated on an external shell (SST-type) by the intermatrix synthesis (IMS) method, and evaluated for water purification applications.

2. Results and Discussion

2.1. Metal Content and Ion Exchange Capacity of the NCs

Ten NC materials were synthesized by following the protocol detailed in the Experimental Section on granulated cation exchange polymeric matrices. The polymeric matrix, the ion exchange capacity (IEC; see Experimental Section), the concentration of ionic precursor and the metal content (determined by induced coupled plasma atomic emission spectrometry, ICP-AES; see Experimental Section) is included in **Table 1**. The metal content was corrected according to the IEC of each raw material, which is indicative of the number of functional groups present in the polymeric matrix.

The metal content in the samples was analyzed considering: 1) the concentration of ionic precursor in the solution, 2) the nature (sulfonated or carboxylated matrices), and 3) the distribution (homogeneous, C-type, or concentrated on an external shell, SST-type) of the functional groups in the polymeric matrix. According to the ICP-AES data, the metal content increased when increasing the precursor concentration in the solution during the loading step. Particularly, the Ag amount in samples loaded with 0.1 M $AgNO_3$ (samples A and F) was at least 5 times higher than in those of the same nature loaded with 0.01 M $AgNO_3$ (samples B and G, respectively). Therefore, a 10 times increase of the ionic precursor concentration only increased 5 times the Ag content. This fact suggested a big excess of the precursor concentration and for economical reasons, from that point, all NC samples were prepared with 0.01 M $AgNO_3$.

Table 1. Polymeric matrix, IEC, concentration of ionic precursor (Ag^+ and Co^{2+}), and metal content (from ICP-AES) of the nanocomposite materials synthesized in this work.

Sample	Matrix	IEC [meq/g]	$[Ag^+]$ [M]	$[Co^{2+}]$ [M]	Ag content [$mmol_{Ag}$/meq]	Co content [$mmol_{Co}$/meq]
A	C100E	2.3	0.1		0.254	
B			0.01		0.064	
C			0.01	0.01	0.069	0.061
D	SST80[a)]	4.2	0.01		0.053	
E			0.01	0.01	0.053	0.073
F	C104E	6.0	0.1		0.054	
G			0.01		0.010	
H			0.01	0.01	0.011	0.017
I	SST104[a)]	7.2	0.01		0.010	
J			0.01	0.01	0.010	0.017

[a)]SST is shallow shell technology.

Regarding the nature of the polymeric matrix, sulfonated NCs presented metallic silver and cobalt amounts between 5 and 6 times higher than carboxylated NCs (as shown when comparing samples A, B, C, D, and E, with, respectively, F, G, H, I and J), probably due to differences in the accessibility to the functional groups during the loading step. The number of functional groups accessible may be influenced by the own nature of the functional groups (strong or weak), functional groups distribution in the polymer and the matrix porosity. This accessibility differences were evaluated by determining the percentage of accessible functional groups in the matrix after and before NPs synthesis by IEC, as detailed in the Experimental Section. The percentage of accessible functional groups varied from 88% for sulfonated polymers to 62% for carboxylated ones. This coincided with the higher metal content observed in sulfonated matrices (see Table 1).

After each loading-reduction cycle these accessible functional groups were completely regenerated and could be loaded with another ionic precursor without interference of the previous metal particles. This fact was demonstrated by ICP-AES since the Ag content in samples B, D, G, and I was, respectively, the same as that obtained in samples C, E, H, and J, which already presented Co-NPs in their structure. Finally, no differences were observed when comparing the metal content between C-type polymers (samples B,C and G,H for sulfonated and carboxylated, respectively), and SST-type polymers (samples D,E and I,J, respectively).

2.2. Distribution and Size of the Metal NPs in the NC

The distribution of metal NPs (MNPs) in the NC was determined using scanning electron microscopy (SEM) coupled

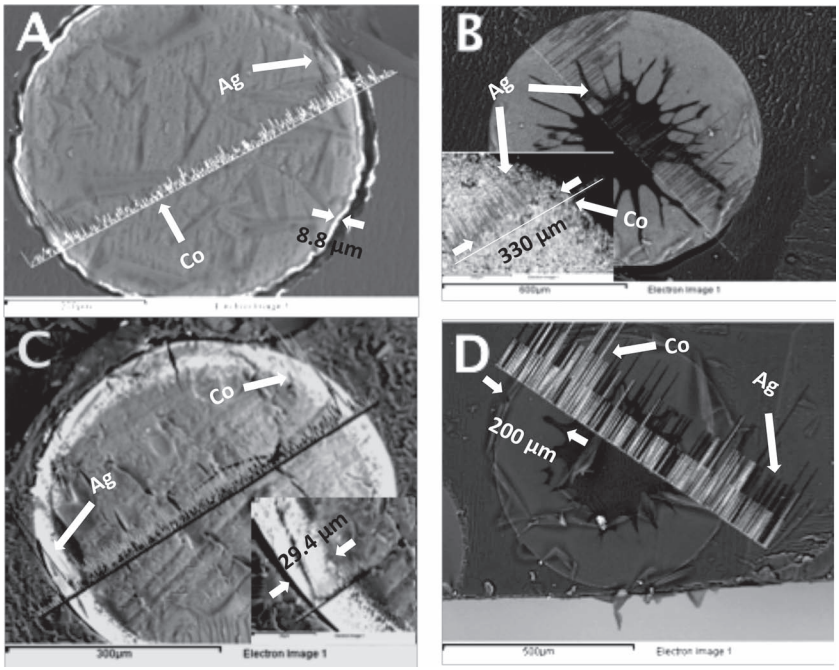

Figure 1. SEM images and EDS spectra for A) sample C (Ag@Co C100E NC) (penetration: 8.8 µm); B) sample E (Ag@Co SST80 NC) (penetration: 330 µm); C) sample H (Ag@Co C104E NC) (penetration: 29.4 µm); and D) sample J (Ag@Co SS104 NC) (penetration 200 µm). In all images, dark grey lines and light grey lines correspond, respectively, to Ag and Co metal distributions in the polymer.

with an energy-dispersive spectrometer (EDS) as detailed in the Experimental Section. **Figure 1** shows representative SEM images and EDS spectra for cross-sections of polymeric beads of the four Ag@Co NCs under study (samples C, E, H, and J).

In all cases, MNPs (white area) were mainly found concentrated on the NC surface. This distribution did not exactly coincide with that reported by fibrous materials.[13]

In that case, although more concentrated in the external region, MNPs were found distributed along the whole cross-section of the NC. The limited access of the ionic metal precursors to the inner functional groups of the granulated resin was associated to diffusion processes related to the low porosity of the material and the Donnan exclusion effect.[14] That is, the negative charge of the material impeded a deep diffusion of the negatively charged ionic reducing agent in the polymer matrix.

Besides, NPs distribution on granulated polymers depended on the functional groups distribution in the polymeric matrix. Matrices with a homogeneous distribution of the functional groups (C100E and C104E) presented NPs in a very thin and superficial metal layer (10–30 µm depth maximum). Conversely, MNPs were more deeply distributed (200–300 µm depth) when the functional groups were concentrated in an external shell (SST80 and SS104). This could be understood by considering the functional groups density (number of functional groups per area unit) of each type of matrix. The functional group density of each material was evaluated as the number of functional groups of each material, determined by acid-base titration (see Experimental Section), per area. In this sense, SST-type materials, with a smaller area since the functional groups were concentrated in an external shell, always presented a higher number of functional groups in their structure and consequently, a higher density. This fact should benefit the loading of the polymer structure with the ionic metal precursor.

The average Ag- and Ag@Co-NPs size was determined by transmission electron microscopy (TEM) images (as detailed in the Experimental Section). More than 100 isolated NPs located far from the NC border (to avoid aggregates[15]) were analyzed in each case. **Figure 2** illustrates an example of Ag@Co-C100E cross-section containing representative isolated core-shell NPs suitably labelled. The size of each particle, oscillating between 25 and 40 nm, was also included in a table inset. A magnification of the image demonstrating the core-shell structure of the NPs was also included inset.

Ag-NPs (13 nm, average) were found to be much smaller than Ag@Co-NPs, which oscillated from around 21 nm for carboxylated matrices to almost 30 nm for sulfonated materials. These core-shell particles were also much bigger than those synthetized following a similar IMS protocol on fibers (16 nm, average).[13] These differences may be due to diffusional processes, particularly to porosity and to the Donnan exclusion effect,

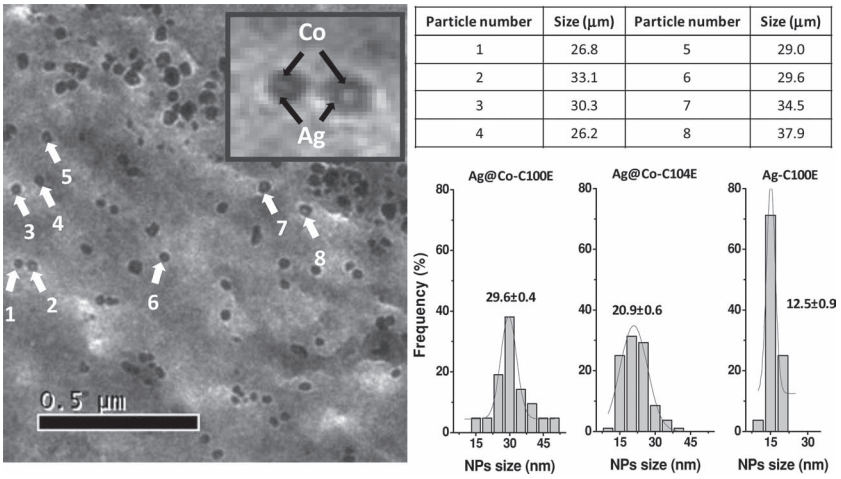

Particle number	Size (µm)	Particle number	Size (µm)
1	26.8	5	29.0
2	33.1	6	29.6
3	30.3	7	34.5
4	26.2	8	37.9

Figure 2. TEM image of Ag@Co-C100E NC cross-section containing Ag@Co-NPs. Inset: an image magnification demonstrating the core-shell structure of the NPs. In the picture, 8 representative Ag@Co-NPs were suitably labeled and their size is included in the table inset. The histograms corresponding to Ag- and Ag@Co-NPs in C100E and Ag@Co-NPs in C104E are also added.

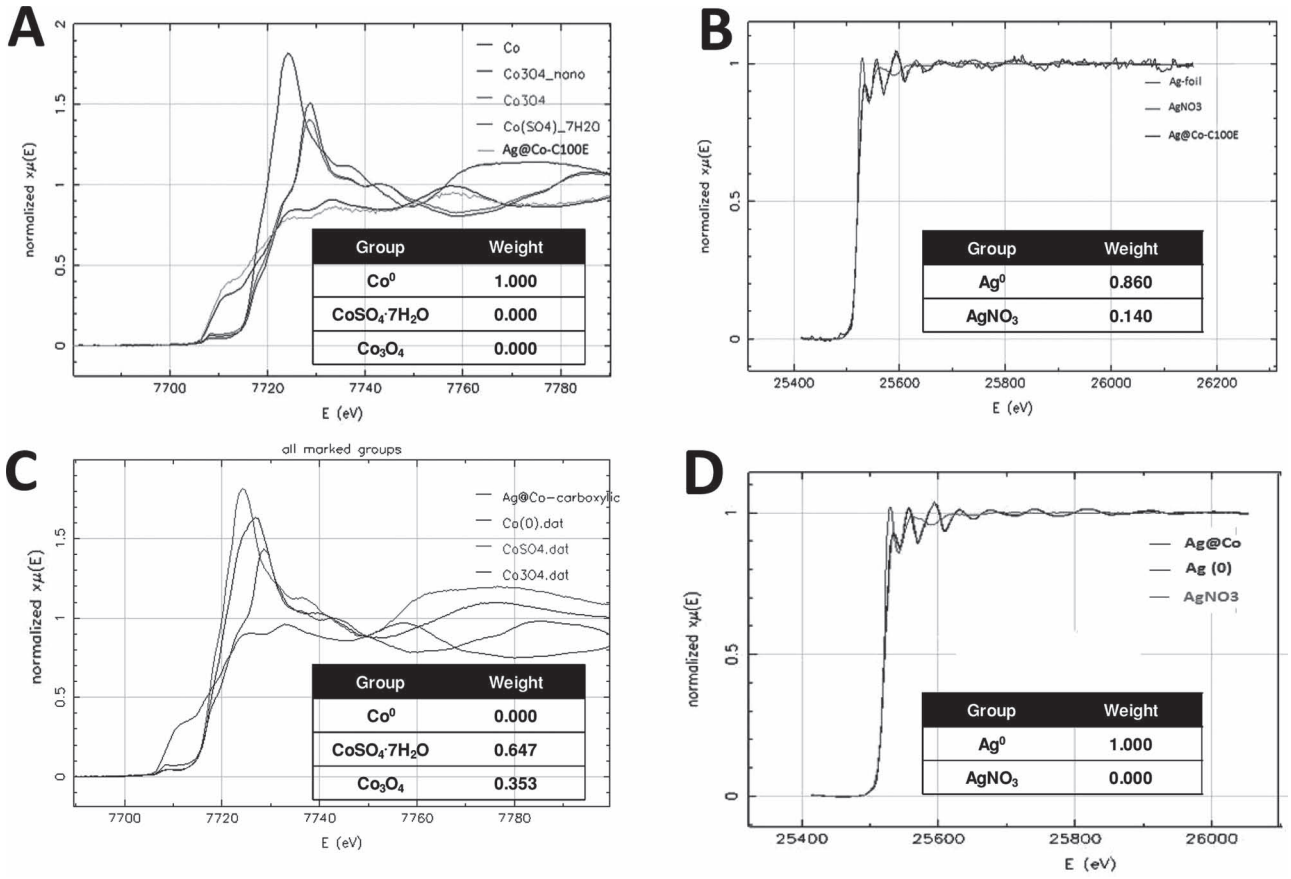

Figure 3. XANES spectra of Ag@Co-NPs in C100E and comparison with A) Co and B) Ag standards. XANES spectra of Ag@Co-NPs in C104E and comparison with C) Co and D) Ag standards. The linear combination fitting among all of the compounds analyzed is also shown inset in a fitting range from –30 to 90 eV (for Co standards) and –20 to 30 eV (for Ag standards).

that may limit the access of the ionic precursors and reducing agents to the functional groups.

2.3. NP Composition, Magnetic Properties, and Antibacterial Activity

The composition and oxidation state of the Ag@Co-NPs components was determined by comparison with Co and Ag standards using X-ray absorption near edge structure (XANES) (Experimental Section). The line spectra corresponding to the Ag@Co-NCs and each Co and Ag standard are illustrated in **Figure 3**. Standard elements spectra were linearly combined and fitted with the sample in order to determine the oxidative state of each element in the sample. The linear combination results are also included (normalized) inset.

The Co spectra for Ag@Co-NPs depended on the matrix. When compared with standards, Ag@Co-NPs in sulfonated matrices showed an average Co spectrum similar to that recorded by the Co^0 standard (Figure 3A). In fact, linear combination fitting results confirmed that all the Co present in that sample was Co^0. Conversely, the Co-core in carboxylated Ag@Co-NCs (Figure 3C) was mainly constituted by a combination of Co^{2+} and Co_3O_4 (65% Co^{2+}, 35% Co_3O_4). Although still not completely demonstrated, the oxidation of the Co core may be due to the small thickness of the Ag shell layer, which may not protect Co from oxidation. In fact, as previously observed, Ag@Co-NPs on sulfonated matrices were almost 10 nm bigger than those synthesized on carboxylated ones.

The different oxidative state of the Co-core may also affect the magnetic properties of the NPs. Co-, CoO- and Co_3O_4-NPs have been reported to present magnetic properties (superparamagnetic for Co-NPs and antiferromagnetic for CoO- and Co_3O_4-NPs).[16] The hysteresis loops of both NCs at 300 K were determined, as described in the Experimental Section, using a superconducting quantum interference device (SQUID) and are plotted in **Figure 4**.

Both materials presented a superparamagnetic behavior with low or null remanent magnetization (*Mr*, the magnetization of the material in absence of external magnetic field) and coercivity (*Hc*, the intensity of the external magnetic field that reduces the magnetization of the material to 0) and with magnetic saturation (*Ms*) above 1500 Oe. As expected, sulfonated materials, with a Co^0-core, showed higher magnetic saturations (14.8 emu/g of Co) than carboxylated NCs (5.3×10^{-3} emu/g of Co) containing Co^{2+}/Co_3O_4-cores.

In the case of Ag, in both polymeric matrices Ag@Co-NPs were principally composed of Ag^0 (86% Ag^0 and 14% Ag^+ for

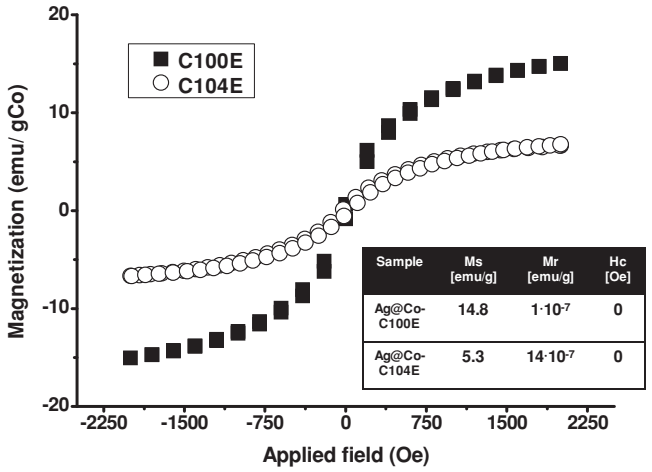

Figure 4. SQUID hysteresis curve of (■) Ag@Co-C100E NC and (○) Ag@Co-C104 NC. The magnitude of the magnetic saturation (*M*s), remanent magnetization (*M*r), and coercivity (*H*c) of each material are included in the table inset.

sulfonated and 100% Ag^0 for carboxylated materials). This slight difference in the composition of the Ag-shell may affect the antibacterial activity of the NCs. In this sense, it is important to remark that, although the antibacterial mechanism of Ag is currently poorly understood, it is thought to be caused by the interaction of metallic Ag and Ag ions with different cell targets.[17] The electron transport chain proteins, the DNA strains or several elements composing the cell wall are some of the identified targets.[17,18] Considering the high stability of the NPs in the polymeric matrix, a contact killing mechanism involving the interaction of the NPs retained in the NC with proteins of the outer structures of the cell seemed to be the most plausible. The contact killing mechanism was demonstrated by comparing the number of life and dead cells attached on the surface of the NCs with and without NPs by fluorescence microscopy (Experimental Section). Fluorescence microscopy images showed that whereas cells attached on the raw material remained alive, most of them died when attached on NCs containing NPs (Figure S.I.1, Supporting Information). The antibacterial activity of each NC was evaluated using the minimum inhibitory concentration (MIC) test, as detailed in the Experimental Section. MIC results are plotted in **Figure 5**. The MIC_{50} values will be expressed as number of NC beads (or polymer particles) in 200 µL of culture medium (beads/200 µL).

Sulfonated and carboxylated NCs presented different behaviours. The raw sulfonated material did not present bactericidal activity in the concentration range under test. However, it became antibacterial when modified with NPs. In the case of sulfonated matrices, Ag@Co-NCs, with a MIC_{50} around 4 beads/200 µL, were found much more bactericidal than Ag-NCs (MIC_{50} between 13–16 beads/200 µL) with the same Ag content. The reasons for that enhancement of antibacterial activity are still controversial, although the oxidative state of the Co in the core of the NP (Co^0) is thought to play a critical role in that. Considering this, the enhancement may be produced by a redox process where the Ag^0-shell oxidized to Ag^+ by contact with bacteria may be quickly reduced to Ag^0 by the Co^0-core, maintaining the structural stability (and activity) of the NPs. Considering the standard reduction potential of both species ($E^0(Ag^+/Ag)$ = 0.80 V and $E^0(Co^{2+}/Co)$ = –0.27 V), this process should be thermodynamically favourable. However, it should be noted that these reduction potentials were only estimative since, as already reported,[19] they usually shifted to more negative values for metal NPs. Note that in this case there were not significant differences between C-type and SST-type materials.

In the case of carboxylated materials, all NCs (even the raw material) showed similar bactericidal activity, probably due to pH changes and not to the presence of antibacterial compounds. For this reason, the MIC test data was not considered in the evaluation of the bactericidal activity of the carboxylated NCs.

The bactericidal activity of the NCs was also evaluated under fluidic conditions following the protocol detailed in the Experimental Section. Bacterial suspension containing 10^5 colony forming units per mL (CFU/mL) were forced to pass though chromatographic columns containing NC material for 1 h under recirculation regime. Bacterial suspensions after crossing the column were regularly extracted (every 10 min) under sterile conditions and the number of viable cells was determined by plating as described in the experimental section. The antibacterial activity of each NC was calculated as the difference between the number of viable cells after and before crossing the NC, in percentage terms. Results corresponding to each NC are plotted in **Figure 6**.

Huge differences were observed between the raw materials and the synthesized NCs when operating under recirculation regimes. At this low contact times, raw materials were not found antibacterial, showing cell viabilities always higher than 65%. In fact, the decrease recorded after 30 min of operation may be associated to bacterial retention in the raw material structure, as already demonstrated by fluorescence microscopy (Figure S.I.1, Supporting Information). In opposition, all NCs showed high antibacterial activity, reducing the bacterial viability to 0% after short recirculation times. Some small differences could also be observed between NCs. That is, C-type NCs always showed slower antibacterial kinetics than SST-type material probably due to a better distribution of NPs in the case of SST-type NCs. Additionally, sulfonated materials always showed faster kinetics probably for the higher Ag amount present on them. Finally, and as already observed in the MIC assays, Ag@Co-NCs presented an enhanced antibacterial kinetic when compared with Ag-NCs, which may be caused by a synergic effect associated to the presence of the Co-core.

2.4. Stability and Long-Term Performance of the NCs

Stability was initially evaluated in terms of metal release. Ag and Co release from Ag@Co-NCs after 60 min of continuous operation was determined by ICP-MS. All samples showed values below 1.0 ppm for Ag and 0.1 ppm for Co. Additionally, differences were obtained when comparing NCs with different nature or distribution of the functional groups. In this sense, the release from carboxylated matrices was much more abundant

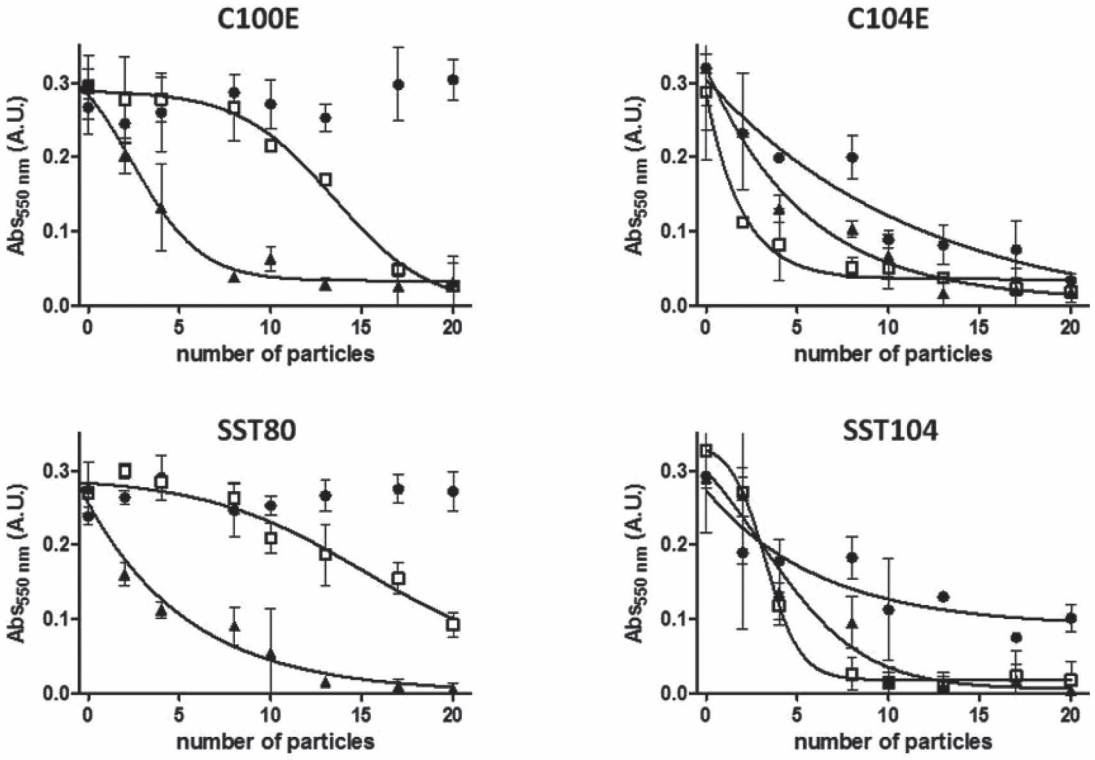

Material	MIC_{50} [particles/ 200 μL]	Material	MIC_{50} [particles/ 200 μL]
C100E	-	C104E	8.9
Ag-C100E	13.4	Ag-C104E	2.2
Ag@Co-C100E	4.1	Ag@Co-C104E	6.0
SST80	-	SST104	10.2
Ag-SST80	16.2	Ag-SST104	4.4
Ag@Co-SST80	4.3	Ag@Co-SST104	5.2

Figure 5. MIC test for the NCs under study. In each case, the absorbance magnitude at 550 nm is represented versus the NC amount (number of beads) for ●) the raw material, □) the Ag-NC, and ▲) the Ag@Co-NC ($n = 3$). The MIC_{50} of each NC is included in the table inset.

(close to 10 times) than that obtained from sulfonated materials with a higher metallic content ($Ag_{SST80} = 0.087/Co_{SST80} = 0.000$ and $Ag_{SST140} = 0.934/Co_{SST140} = 0.004$). This may be associated to the different oxidative state of the Co-core in the NC. As previously exposed, sulfonated Co^0-cores could re-reduce the Ag shell preserving the integrity (and activity) of the NPs. It was not possible with the Co^{2+}/Co_3O_4-core of the carboxylated NCs. Considering the functional groups distribution, C-type matrices showed a higher release than SST-type with similar metallic content ($Ag_{C100E} = 0.563/Co_{C100E} = 0.002$ and $Ag_{SST80} = 0.087/Co_{SST80} = 0.000$). In this case, both the higher functional groups density in the external matrix and the deeper NPs distribution may benefit the stability of the NPs on the SST-type NCs, reducing the metal release.

On the other hand, the antibacterial performance of the NCs was evaluated under fluidic conditions. In this case, the recirculation protocol described in Section 2.3 was repeated weekly during 5 consecutive weeks in order to evaluate the long term performance of the NCs. The antibacterial activity of each NC was this time calculated as the difference between the number of viable cells crossing the NC with and without NPs, in percentage terms. The antibacterial activity of both sulfonated and carboxylated NCs was found to decrease from 90% to around 70% after 5 weeks of continuous operation (Figure S.I.2, Supporting Information). Therefore, these NCs showed good performance and stability even under continuous flow operation, which coincided with the low metal release previously observed.

2.5. NC Cytotoxicity

Cytotoxicity assays were performed by using the MTT (3-(4,5-dimethylthiazol-2-yl)-2,5-diphenyltetrazolium bromide)

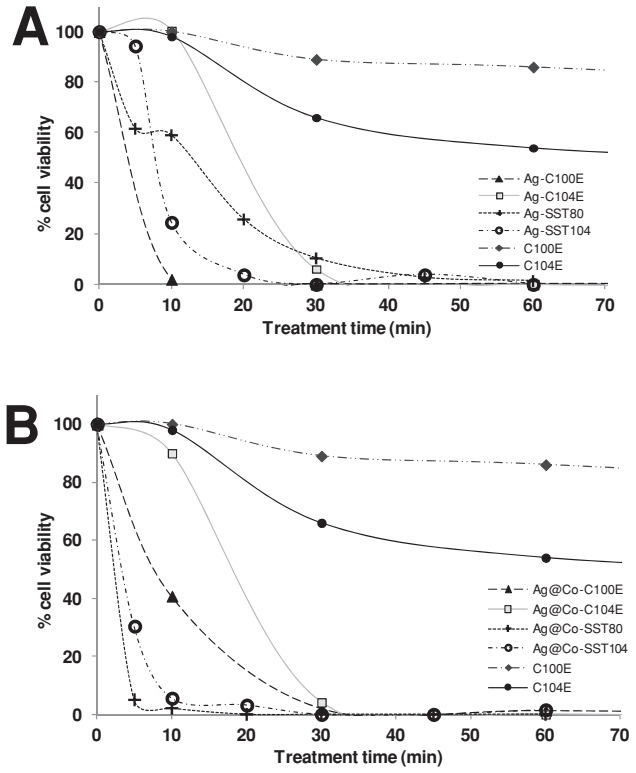

Figure 6. Representation of the variation of the number of viable cells in percentage terms (% cell viability) versus treatment time for A) Ag- and B) Ag@Co-NCs. Raw materials are also included as control.

assay detailed in the Experimental Section. **Figure 7** illustrates the cell viability after 24 h of treatment of vascular smooth muscle cells (VSMC) with 1 and 5 beads of raw material, Ag-NCs and Ag@Co-NCs.

Considering sulfonated samples, only Ag@Co-NCs showed cytotoxicity, with a decrease of the cell viability close to 50% after 24 h incubation with 5 NC beads. This result was in concordance with the already reported cytotoxic activity of Co.[20] Thus, some Co could be released from the NC structure after 24 h incubation, producing cytotoxicity.

In contrast, carboxylated matrices always evidenced cytotoxic effects. This was again associated to pH changes. In this case, pH changes were evidenced by the presence of a pH indicator in the culture medium. The culture medium colour, initially red for the presence of the deprotonated form of the pH indicator (phenol red), changed to yellow (protonated form) indicating an acidification of the medium. This acidification could clearly have cytotoxic effects.

In summary, matrices containing sulfonated functional groups, and particularly those where the functional groups are concentrated in an external shell (SST-type), are advantageous for water purification applications for presenting elevated metal amounts, an enhanced antibacterial activity and high stability since they have the lowest metal release.

3. Conclusions

Superparamagnetic Ag@Co-NCs with a low-cost magnetic Co-core and an antibacterial Ag shell have been fabricated by IMS under soft reaction conditions on sulfonated and carboxylated granulated cation exchange polymeric matrices for water purification applications. The nature of the functional group and their distribution on the matrix (homogeneous, C-type, or concentrated in an external shell, SST-type) modified the NC properties and activity. Sulfonated NCs (independently on being C- or SST-type) presented higher metal amounts (around 5 times higher) and bigger NPs size (close to 10 nm bigger) than carboxylated ones. The differences in metal content affected the

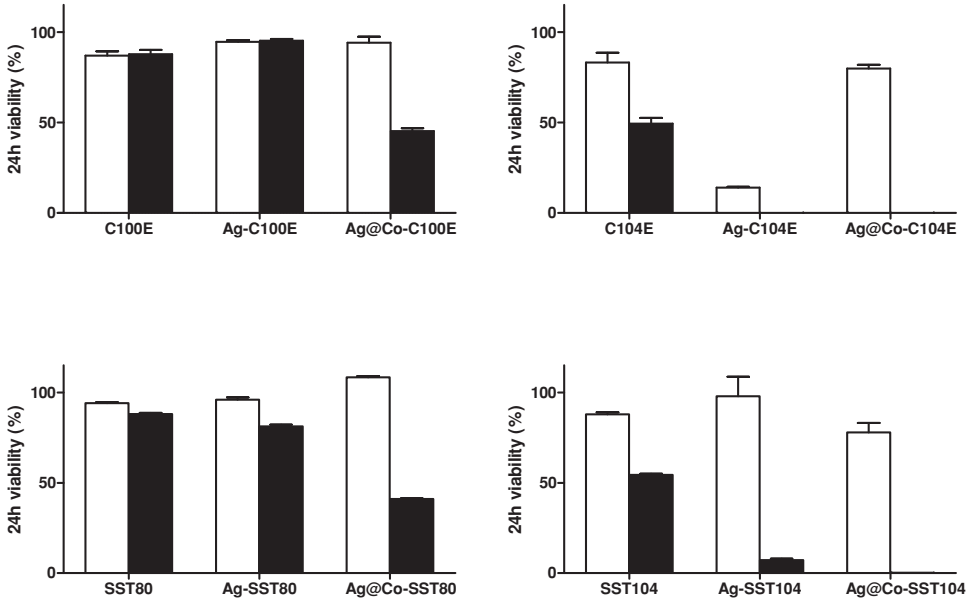

Figure 7. MTT cytotoxicity assay for the NCs under study. Cell viability was determined after 24 h of incubation with 1 (white) and 5 (black) NC beads ($n = 3$). Viability was expressed as percentage versus non-treated control samples.

NPs composition and activity. Thus, the thin Ag layer on carboxylated NCs was not enough to preserve the oxidative state of the Co-core, which oxidised to a mixture of Co^{2+} and Co_3O_4 with antiferromagnetic properties. Conversely, the Co-core in sulfonated NCs maintained their Co^0 oxidative state and their superparamagnetic properties. The Co-core oxidative state also influenced the integrity of the NPs and the antibacterial activity of the NC. Thus, sulfonated Ag@Co NCs presented lower metal release than carboxylated ones and an enhanced antibacterial activity when compared with Ag-NCs with a similar Ag content. Both aspects were associated to the spontaneous reduction of the oxidised Ag (oxidised by contact with bacteria) by Co^0. Sulfonated materials also presented faster antibacterial kinetics and especially SST-type NCs. Besides, metal release in SST-type NCs, with a higher density of functional groups in their external structure and a deeper distribution of NPs, was lower than in C-type structures. Thus, SST-type sulfonated matrices would be the best alternative for the synthesis of Ag@Co-NCs on granulated cation exhange polymers with antibacterial and superparamagnetic activity.

4. Experimental Section

Materials: Metal salts $Co(NO_3)_2{\cdot}6H_2O$ and $AgNO_3$, $NaBH_4$ and NaCl (all from Aldrich, Germany) and HNO_3 (Panreac S.A, Spain) were used as received. Solutions were prepared in MiliQ water. Granulated cation exchange materials were kindly supplied by PUROLITE Iberia S.A. Most relevant properties of the raw materials (provided by the supplier) are summarized in Table S.I.1 (Supporting Information).

Synthesis of Metallic Nanoparticles in the Polymeric Matrix: The raw material was initially pre-treated with 0.1 M NaCl (sulfonated materials) or 0.1 M NaOH (carboxylated materials) for 1 h to ensure the complete Na^+-form of the functional groups. After washing with deionized water (3 times), the raw material beads were dried (24 h at 80 ºC) and sieved to homogenize the bead size between 400 and 500 µm. The synthesis of the MNPs in the polymeric matrix was carried out using a variation of the IMS protocol already reported[12b,21] and briefly described below. In the synthesis of Ag-monometallic NPs, the cation exchange polymeric matrix was loaded with Ag^+ cations by incubation with $AgNO_3$ (0.1 or 0.01 M) for 1 h under stirring. After washing with deionised water, the Ag^+ cation was subsequently reduced to Ag^0 after reaction with 0.5 M $NaBH_4$ for 1 h. Similarly, in the case of Ag@Co bimetallic NPs, Co-NPs were synthesized by loading of the raw material with 0.01 M $Co(NO_3)_2$ for 1 h and reduction of the Co^{2+} ions to Co^0 after reaction with 0.5 M $NaBH_4$. Next, the material containing Co-NPs was loaded with 0.01 M $AgNO_3$ solution for 30 min and the Ag^+ was reduced to Ag^0 by addition of 0.5 M $NaBH_4$. Core-shell Ag@Co bimetallic NPs were thus obtained in the polymeric material structure.

ICP-AES and ICP-MS Measurements: The concentration of metal retained in the polymeric matrix was determinate by ICP–AES using an Iris Intrepid II XSP spectrometer (Thermo Electron Co.). Experimentally, 5.0 mg of each polymeric structure were introduced in 1 mL of concentrated nitric acid and incubated between 5–10 h to ensure the metal oxidation. Before the analysis, the solution was diluted 25 times with deionised water and filtered using 0.22 µm Millipore filters to eliminate non-dissolved particles. Once measured, metal concentration of each sample was obtained by comparison with certified standard solutions of both elements (JT Baker). Wavelengths with good sensitivity and without interference were chosen. The instrumental average uncertainty of the determination was always found lower than 2%.

The ICP-MS detector (ICP-MS Agilent 7500) was used for the determination of metal leaking from the polymeric matrix. In this case, samples were prepared as detailed above but, due to the lower detection limit of the technique, after treatment with concentrated nitric acid, samples were diluted 50 times with deionised water at the clean room facilities. The instrumental average uncertainty was again lower than 2% for all the samples.

Ion Exchange Kinetics Evaluation: The ion exchange kinetics of these materials was evaluated by acid-base tritation. Particularly, it is determined by monitoring the amount of Ca^{2+} ions exchanged with the cations initially retained in the NC structure. Experimentally, 50 mL of a 100 ppm Ca^{2+} solution were forced to pass through a chromatographic column (0.5 cm diameter, 0.3 cm length) already containing 0.4 g of NC at a contant flow rate of 1 mL/min. At regular times, 1 mL aliquots were extracted and diluted 10 times with deionized water. The Ca^{2+} concentration in the aliquot was determined by ICP-AES.

Scanning and Transmission Electron Microscope Imaging: SEM coupled with EDS (Zeiss EVO MA 10) was used to obtain the metal concentration profiles along the cross-section of the NCs described in above. TEM imaging (JEOL 2011, Jeol Ltd.) was used to characterize the size, morphology and distribution of the MNPs along the polymeric structure. Before the microscopic examination, samples were embedded in an epoxy resin and cross-sectioned with a Leica EM UC6 Ultramicrotome using a 35° diamond knife (Diatome).[22]

X-Ray Absorption Near Edge Structure Analysis: XANES technique supplies information related to atomic organization and chemical bonding by comparison (linear combination) with standards. In this case, XANES was used to determine the oxidation state of Ag- or Ag@Co-NPs synthesized on the polymeric matrices detailed in Table 1. Co^0, $CoSO_4{\cdot}7H_2O$, Co_3O_4, Ag^0 and $Ag(NO_3)$ were used as standards to calibrate the energies of the edge positions for Ag and Co at different environments. NCs containing Ag or Ag@Co-NPs were mounted in aluminum cells and sealed with a polyimide tape (KAPTON-500H, 125 µm thickness). Co K-edge and Ag L-edge X-ray absorption spectra were recorded on the BM25A beam line of the ERSF synchrotron source (Grenoble, France) in transmission mode, under nitrogen/argon atmosphere (85:15) and at room temperature. Absorption spectra were analyzed and modeled using the ATHENA and the ARTEMIS software developed by Ravel and Newville.[23]

Magnetic characterization: SQUID, at the Institut de Ciències dels Materials de Barcelona (ICMAB, CSIC) was used to determinate the magnetic properties of the NCs. The SQUID is a very sensitive magnetometer used to measure extremely weak magnetic fields, based on superconducting loops containing Josephson junctions. In this case, 5 mg samples were accurately introduced in suitable test tubs and the magnetization was analysed at room temperature. A SQUID MPMS-XL7 at 300 K and working between 0 and 7 T of magnetic field intensity was used.

Antimicrobial Tests: *Escherichia coli* (*E. coli*, CGSC 5073 K12) and *Pseudomona putida* (*P. putida*, KT2442) cultures were provided by the Department of Genetics and Microbiology of the Universitat Autònoma de Barcelona (UAB). Luria-Bertani (LB) and AB minimal medium (ABMM, composition in 1 L:2 g $[NH_4]_2SO_4$, 7.3 g Na_2HPO_4, 7.8 g KH_2PO_4, 3 g NaCl, 0.011 g Na_2SO_4, 0.2 g $MgCl_2{\cdot}6H_2O$, 3.6 mg $CaCl_2$, 0.2 mg $FeCl_3{\cdot}6H_2O$, supplemented with 0.02 M glucose as the carbon source) were used for the antibacterial activity tests. Two tests were performed to evaluate the antibacterial activity of the NC: the MIC test and continuous flow analysis. Additionally, NC samples were analyzed using fluorescence microscopy as detailed below.

MIC Assay: The MIC_{50} is defined as the concentration of an antimicrobial agent that inhibits the proliferation of 50% of the microorganisms presents in a sample. In this case, the MIC_{50} of each material was determined by introducing an increasing amount of NC in individual wells of a 96-well ELISA plate already containing 200 µL of 10^5 colony forming units per mL (CFU/mL) of *E. coli* in LB medium. After overnight incubation (16 h), bacterial proliferation was evaluated by measuring the optical density of each well at 550 nm using a SmartSpec Plus Spectophotometer (Biorad). The antibacterial activity of the monometallic Ag and bimetallic Ag@Co NCs was determined. The raw material without NPs was used as control.

Antibacterial Kinetic Test: The antibacterial activity of the NC was also evaluated under fluidic conditions. Experimentally, 0.4 g of NC were introduced in an ion exchange column (0.5 cm diameter, 3 cm length). The column was connected to a peristaltic pump that allowed the control of the flow rate. Bacterial samples containing 10^5 CFU/mL of *P. putida* in AB minimal medium (ABMM) were forced to pass through the column at a flow rate of 1 mL/min. The fluidic system operated in a recirculation regime where the initial bacterial suspension was recirculated through the column for the duration of the experiment (see Figure S.I.3, Supporting Information). Filtrate aliquots were regularly extracted and cultured on agar plates containing LB. Bacteria concentration was determined by counting the number of colonies after overnight incubation at 37 °C.

Fluorescence Microscopy: Fragments of Ag@Co-NC material and the raw material without NPs, used as control, were incubated overnight with a bacterial suspension containing 10^9 CFU/mL of *E. coli*. In both cases, the material was initially rinsed with phosphate buffered saline (PBS, pH 7) and stained using the Live/Dead Invitrogen Kit *Bac*Light (Invitrogen) by following the protocol detailed by the supplier. The material was incubated in the staining solution containing the suitable concentration of the two nucleic acid stains, propidium iodide (component A) and SYTO (component B). SYTO could penetrate both live and dead cells whereas propidium iodide could only penetrate damage membranes, reducing SYTO fluorescence and staining dead cells. Both stains were excited at 470 nm but emitted at different wavelengths. Thus, propidium iodide, which emitted at 630 nm, stained dead cells with red fluorescence and SYTO that emitted at 530 nm, stained live cell with green fluorescence. After 20 min of incubation, a drop of the component C (immersion oil) was added to the NCs, which were fixed in a glass slide by covering them with a cover slip and sealing. Images were acquired with a Zeiss AXIO Imager A1 fluorescence microscope containing a 470 nm excitation laser and suitable filter sets. Images were acquired using a 40× magnification objective at acquisition times that differed depending on the sample and on the staining molecule.

Cytotoxicity Assay: Determination of cell viability is a common method to estimate biocompatibility of materials. The cytotoxicity of the particles was evaluated in vascular smooth muscle cells cultured from rat aorta[24] by using the colorimetric MTT (3-(4,5-dimethylthiazol-2-yl)-2,5-diphenyltetrazolium bromide) assay. This technique is based on the ability of viable cells to transform the MTT salt into formazan dyes. VSMCs were tripsinised and plated at 7×10^4 cell/well in a 96-well culture plate containing Dulbecco's modified Eagle's medium (DMEM) (Gibco-Invitrogen, Spain) and were maintained for 24 h to attach. After a 24 h incubation period with the beads (1 and 5 beads), the medium containing the samples was aspirated, the wells were washed with PBS and the MTT solution (1 mg/mL) was added and incubated for 4 h. The purple formazan generated by viable cells was solubilised with 20% sodium dodecyl sulphate in 0.02 M HCl and incubated for 10 h at 37°C. The optical density of each well was determined at 540 nm in a Thermo Electron Multiskan EX plate reader (VWR International, Pennsylvania). Cell viability was expressed as percentage in relation to controls (non-treated cells).

Supporting Information

Supporting Information is available from the Wiley Online Library or from the author.

Acknowledgements

This work was supported by Research Grant MAT2006-03745, CSD2006-00044 TRAGUA (CONSOLIDER-INGENIO-2010) and CTQ2009-14390-C02-02 from the Ministry of Science and Technology of Spain and by ACC1Ó for VALTEC 09-02-0057 Grant within FEDER Program. A.A. also acknowledge the FI (AGAUR). X.M.-B. acknowledges the Spanish Ministry of Science and Education for the award of a Ramon y Cajal contract. Special thanks are given to Servei de Microscopia from Universitat Autònoma de Barcelona, the Institut de Ciències dels Materials from Barcelona (CSIC), Centro de Investigación, Tecnología e Innovación de la Universidad de Sevilla (CITIUS) and the ERSF Synchrotron (Grenoble, France) to carry out the Project: "Speciation of Ag@Co and Pd@Co nanoparticles synthesized in polymeric matrix by XAS".

Received: September 14, 2012
Published online: December 7, 2012

[1] M. A. Shannon, P. W. Bohn, M. Elimelech, J. G. Georgiadis, B. J. Marinas, A. M. Mayes, *Nature* **2008**, *452*, 301.
[2] a) M. Montgomery, M. Elimelech, *Environ. Sci. Technol.* **2007**, *4*, 17; b) P. Singh, L. Bengtsson, *J. Hydrol.* **2005**, *300*, 140.
[3] T. P. Barnett, J. C. Adam, D. P. Lettenmaier, *Nature* **2005**, *438*, 303.
[4] H. Organization, *Emerging Issues in Water and Infectious Disease*, World Health Organization, Geneva **2003**.
[5] a) J. G. Pressman, S. D. Richardson, T. F. Speth, R. J. Miltner, M. G. Narotsky, I. I. I. E. S. Hunter, G. E. Rice, L. K. Teuschler, A. McDonald, S. Parvez, S. W. Krasner, H. S. Weinberg, A. B. McKague, C. J. Parrett, N. Bodin, R. Chinn, C.-F. T. Lee, J. E. Simmons, *Environ. Sci. Technol.* **2010**, *44*, 7184; b) E. M. Smith, M. J. Plewa, C. L. Lindell, S. D. Richardson, W. A. Mitch, *Environ. Sci. Technol.* **2010**, *44*, 8446.
[6] a) H. C. Neu, *Science* **1992**, *257*, 1064; b) J. P. Ruparelia, A. K. Chatterjee, S. P. Duttagupta, S. Mukherji, *Acta Biomater.* **2008**, *4*, 707.
[7] a) M. Rai, A. Yadav, A. Gade, *Biotechnol. Adv.* **2009**, *27*, 76; b) N. Poulter, X. Muñoz-Berbel, A. L. Johnson, A. J. Dowling, N. Waterfield, A. T. A. Jenkins, *Chem. Commun.* **2009**, 7312.
[8] a) L. Yin, Y. Cheng, B. Espinasse, B. P. Colman, M. Auffan, M. Wiesner, J. Rose, J. Liu, E. S. Bernhardt, *Environ. Sci. Technol.* **2011**, *45*, 2360; b) X. Yang, A. P. Gondikas, S. M. Marinakos, M. Auffan, J. Liu, H. Hsu-Kim, J. N. Meyer, *Environ. Sci. Technol.* **2011**, *46*, 1119.
[9] M. Charnley, M. Textor, C. Acikgoz, *React. Funct. Polym.* **2011**, *71*, 329.
[10] K. Varaprasad, Y. M. Mohan, S. Ravindra, N. N. Reddy, K. Vimala, K. Monika, B. Sreedhar, K. M. Raju, *J. Appl. Polym. Sci.* **2010**, *115*, 1199.
[11] S. Ghosh, R. Kaushik, K. Nagalakshmi, S. L. Hoti, G. A. Menezes, B. N. Harish, H. N. Vasan, *Carbohydr. Res.* **2010**, *345*, 2220.
[12] a) J. Liu, Z. Zhao, H. Feng, F. Cui, *J. Mater. Chem.* **2012**, *22*, 13891; b) A. Alonso, X. Muñoz-Berbel, N. Vigués, J. Macanás, M. Muñoz, J. Mas, D. N. Muraviev, *Langmuir* **2011**, *28*, 783.
[13] A. Alonso, N. Vigues, X. Muñoz-Berbel, J. Macanas, M. Muñoz, J. Mas, D. N. Muraviev, *Chem. Commun.* **2011**, *47*, 10464.
[14] F. G. Donnan, *Chem. Rev.* **1924**, *1*, 73.
[15] A. Alonso, X. Muñoz-Berbel, N. Vigues, R. Rodriguez-Rodriguez, J. Macanas, J. Mas, M. Muñoz, D. N. Muraviev, *RSC Adv.* **2012**, *2*, 4596.
[16] A.-H. Lu, E. L. Salabas, F. Schüth, *Angew. Chem. Int. Ed.* **2007**, *46*, 1222.
[17] W. Jung, H. Koo, K. Kim, S. Shin, S. Kim, Y. Park, *Appl. Environ. Microbiol.* **2008**, *74*, 2171.
[18] P. Gajjar, B. Pettee, D. Britt, W. Huang, W. Johnson, A. Anderson, *J. Biol. Eng.* **2009**, *3*, 9.
[19] a) W. J. Plieth, *J. Phys. Chem.* **1982**, *86*, 3166; b) H. C. Choi, M. Shim, S. Bangsaruntip, H. Dai, *J. Am. Chem. Soc.* **2002**, *124*, 9058.
[20] Z. H. Chohan, C. T. Supuran, *J. Enzyme Inhib. Med. Chem.* **2005**, *20*, 463.
[21] D. N. Muraviev, J. Macanás, J. Parrondo, M. Muñoz, A. Alonso, S. Alegret, M. Ortueta, F. Mijangos, *React. Funct. Polym.* **2007**, *67*, 1612.
[22] S. Lenoir, C. Pagnoulle, M. Galleni, P. Compère, R. Jérôme, C. Detrembleur, *Biomacromolecules* **2006**, *7*, 2291.
[23] B. Ravel, M. Newville, *J. Synchrotron Radiat.* **2005**, *12*, 537.
[24] R. Rodriguez-Rodriguez, X. Muñoz-Berbel, S. Demming, S. Büttgenbach, M. Herrera, A. Llobera, *Biomed. Microdevices* **2012**, *14*, 1129.